Check for updates

Lithospheric thinning beneath the Tengchong volcanic field, Southern China: Insight from Cenozoic calc-alkaline basalts

Kefei Chen[1,2], Shaolin Liu[1]*, Dinghui Yang[3], Xiwei Xu[1], Yadong Wu[4], Shuang Yang[5], Shuxin Yang[1] and Haodong Zhang[1]

[1]National Institute of Natural Hazards, Ministry of Emergency Management of China, Beijing, China, [2]Research Institute of Petroleum Exploration & Development, PetroChina, Beijing, China, [3]Department of Mathematical Sciences, Tsinghua University, Beijing, China, [4]State Key Laboratory of Lithospheric Evolution, Institute of Geology and Geophysics, Chinese Academy Sciences, Beijing, China, [5]State Key Laboratory of Nuclear Resources and Environment, East China University of Technology, Nanchang, China

The Tengchong Cenozoic volcanic field lies in SE margin of the Tibetan Plateau. The basalts of the Tengchong field exhibit evident spatial-temporal variations, but consensus on their meaning has not been reached yet. In this study, we collected basalts from western, central and eastern areas in the Tengchong volcanic field and measured the whole-rock and olivine major and trace elements of basalts. Tengchong basalts exhibit remarkable chemical and isotopic diversity, showing a strong correlation with eruption locations and ages. Specifically, basalts in the western and eastern areas (formed at 7.2−2.8 Ma) are characterized by high $^{87}Sr/^{86}Sr$ and low $^{3}He/^{4}He$ ratios, while those in the central area (formed at 0.6−0.02 Ma) feature low $^{87}Sr/^{86}Sr$ and high $^{3}He/^{4}He$ ratios. Based on the temperature- and pressure-dependent elemental partition coefficients, this phenomenon is interpreted as mainly caused by the difference in lithospheric thickness among these areas. On the one hand, the estimated primary magmas in the eastern and western areas show higher SiO_2, Na_2O, $(La/Sm)_N$, Hf/Lu and Ba/Zr ratios than those in the central area. On the other hand, the Ni contents in olivine phenocrysts are higher in the western and eastern areas than in the central area. As different amounts of extension result in different degrees of decompression of the asthenosphere, finally influencing the compositional variation of magmas, these results indicate that the lithosphere in the eastern and western areas is thicker than that in the central area. In addition, basalts erupted in the eastern and western areas are older than those in the central area, suggesting lithospheric thinning. We propose that lithospheric extension due to slab rollback may have caused lithospheric thinning. In addition, according to the different deformation modes of the crust and lithospheric mantle, our study supports mantle-crust decoupling south of ~26°N in SE margin of the Tibetan Plateau.

KEYWORDS

calc-alkaline basalts, olivine, major and trace elements, lithospheric extension, SE Tibet

1 Introduction

Continental basaltic magmatism with temporal-spatial variation is common, and this magmatism can provide valuable insights into the characteristics of the lithospheric mantle and regional tectonic evolution. Continental basalts usually show large variations in compositions and isotopes, which is typically ascribed to mantle heterogeneity. Four models have been

FIGURE 1
Tectonic settings around the Tengchong volcanic field. **(A)** Major tectonic units around the Tengchong volcanic field. The red triangles indicate Quaternary volcanoes in Myanmar and Yunnan, China. The volcano data are from Lee et al. (2016). The black lines delineate the major faults in and near the Tibetan Plateau (Mo et al., 2006). The red rectangle denotes the study area. **(B)** Location of the Tengchong volcanic field and distribution of convergent boundaries and faults in SE margin of the Tibetan Plateau (modified from Zhou et al., 2012). **(C)** Distribution of magmatic rocks from different periods in the Tengchong volcanic field (modified from Cheng et al., 2020). The gray ellipses mark the areas where representative samples were collected. **(D)** Cross-section of line A–B in plot **(C)**, illustrating the variation in lithospheric thickness beneath the Tengchong area (depth of LAB is from Hu et al. (2012), Zhang et al. (2015); Yang et al. (2017)).

proposed to interpret these continental basalt variations. The first model is partial melting of the asthenosphere owing to the thinning and rifting of the continental lithosphere (White, et al., 1987; McKenzie and Bickle, 1988; Tang et al., 2006; Acocella, 2014; Zhang et al., 2021). The second model is decompression melting caused by lithospheric mantle removal and asthenospheric upwelling (Hoernle et al., 2006; Xu et al., 2008; Timm et al., 2009; Zhu et al., 2012). The third model is buoyant upwellings driven by deep subducted slabs (Davies and Bunge, 2006; Chen et al., 2017; Kuritani et al., 2019; Xu et al., 2021). The fourth model is edge-driven convection caused by lithospheric edge associated with plate movement (King and Ritsema, 2000; Dai et al., 2021).

The eastward subduction of the Indian plate and the following India-Asia collision at 55 Ma has resulted in volcanism (8 Ma to present) in SE margin of the Tibetan Plateau. This process results in partial melting of metasomatized mantle sources, and erupted calc-alkaline basalts in the Tengchong terrane (Zhu et al., 1983; Guo et al., 2015). The Tengchong terrane is thought to be the SE extension of the Lhasa terrane (Mo et al., 2006; Figure 1A). The Tengchong volcanic field is located within a pull-apart basin due to WNW–NW extension and NNE–NE compression (Wang et al., 2007; Zhou et al., 2012) (Figure 1). The volcanic rocks in the Tengchong volcanic field show evident temporal-spatial variation. The early erupted basalts (8–2.8 Ma) are mainly distributed in the eastern and western margins of the basin, while basalts that erupted later (0.6–0.02 Ma) are mainly located in the central basin (Cheng et al., 2018). Two main factors are employed to interpret this variation. On the one hand, chemical and geophysical studies suggest that volcanism is closely related to the underthrusting Indian plate (Zhu et al., 1983; Guo et al., 2015; Cheng et al., 2020), and the different degrees of partial melting of metasomatized asthenospheric mantle may result in the temporal-spatial variations of composition and isotope. On the other hand, local tectonic investigation indicates that the Tengchong volcanism was controlled by strong tectonism in SE margin of the Tibetan Plateau (Wang and Burchfiel, 1997; Wang et al., 2007; Wang et al., 2008). The clockwise rotation of Tengchong terrane and strike-slip motion of Sagaing and Gaoligong Faults induced E–W extension (Figure 1B). The extension results in continental rifting and may have led to the obvious geochemical diversity ($^{87}Sr/^{86}Sr$ ranging from 0.7053 to 0.7089) in the Tengchong volcanic field (Wang and Burchfiel, 1997; Cheng et al., 2018; Tian et al., 2018).

Researchers have considered both the subducted slab and continental extension. The subducted slab controlling Tengchong volcanism is revealed by enriched chemical and isotopic signatures (Zhu et al., 1983; Chen et al., 2002; Guo et al., 2015; Cheng et al., 2020). The effect of continental extension on Tengchong volcanism is not well understood (Zhou et al., 2012; Duan et al., 2019). Tengchong basalts feature calc-alkaline characteristics, which can be formed in intraplate areas with continental extension (e.g., Thompson and Gibson, 1994; Hawkesworth et al., 1995; Depaolo and Daley, 2000; Beier et al., 2012). These kinds of calc-alkaline basalts are usually characterized by composition and isotope variations in terms of temporal-spatial distribution. Continental extension usually occurs in rifts, and basalts along rift axes are more sodic and less radioactive than those along rift margins (Thompson and Gibson, 1994). This phenomenon has already been observed in the Basin and Range province of the southwestern United States of America, where the generation of calc-alkaline basalts is closely related to lithospheric extension (Hart et al., 1989; Hawkesworth et al., 1995; Özdemir and Güleç, 2014).

Lithospheric extension results in lithospheric thinning, the process of which controls the composition and isotope variations (Thompson and Gibson, 1994; Hawkesworth et al., 1995; Depaolo and Daley, 2000; Beier et al., 2012). Lithospheric thinning can be detected by several methods. Geophysical studies show that the lithosphere thickness in Tenghcong volcanic field is approximately 80–90 km, and lithosphere in the western and eastern areas is 10 km thicker than that in the central area (Hu et al., 2012; Zhang et al., 2015; Yang et al., 2017). The lithosphere can interfere with the upwelling of hot melt. Lithospheric thinning can form a decompression environment, causing partial melting of the asthenospheric mantle. The variation in lithospheric thickness results in different degrees of decompression, leading to varying extents of partial melting below the lithosphere–asthenosphere boundary. In addition, lithospheric thickness can also affect the temperature- and pressure-dependent elemental partition coefficients (Daley and DePaolo, 1992; Ellam, 1992; Beier et al., 2012; Gale et al., 2014; Niu, 2021). Previous studies have found that the lithospheric thickness and compositional heterogeneity of subcontinental lithospheric mantle play important roles in the composition of generated mafic magmas and olivine (Zhang and guo, 2016; Sun et al., 2017; Guo et al., 2020). The major element contents of basalt and olivine are sensitive to lithospheric thickness, while radioactive isotopes are sensitive to the isotopic composition of the lithosphere. The erupted basalts span the entire period of extension, from the earliest lithospheric extension with the formation of late Miocene basalts, to the present rift basin with the formation of Quaternary basalts (Wang and Burchfiel, 1997). Therefore, analyzing the compositions of basalt and olivine in different periods is helpful for understanding the process of lithospheric thinning in the Tengchong volcanic field.

The Tengchong basalts are suitable for studying extension-related volcanism for two reasons. First, the Tengchong basalts span the entire period of major extension (Wang et al., 2007; Wang et al., 2008). Second, the lithospheric mantle is geochemically distinct from the underlying asthenospheric mantle (Chen et al., 2022). To clarify the effect of continental extension on Tengchong volcanism, we collected basalts from the eastern, central and western areas of the Tengchong volcanic field and analyzed the major and trace elements and Sr–Nd isotopes of basalt, as well as the major and trace elements of olivine. This study may also provide new insights into the origin of the Tengchong volcano and mantle dynamics process of SE margin of the Tibetan Plateau in the Cenozoic.

2 Geological setting

The Tengchong volcanic field is located between the Yangtze plate and Burma Central Lowlands (Figure 1B). Tengchong volcanic field is a monogenic volcanic field, and more than 90 individual cones are recognized (Zhou et al., 2012; Guo et al., 2015). The volcanism in Tengchong field produced approximately 25 craters and associated lava flows, pyroclastic deposits and well-preserved cinder cones (Huangfu and Jiang, 2000). The Tengchong field is within a NE–NNE-trending rift basin, which mainly contains left-lateral faults (Wang et al., 2007; Wang et al., 2008). The distribution of volcanic rock is closely related to the faults (Guo et al., 2015), and volcanic rocks of different types were mainly formed in four periods, i.e., (1) late Miocene-Pliocene basalt, (2) early Pleistocene trachyandesites and
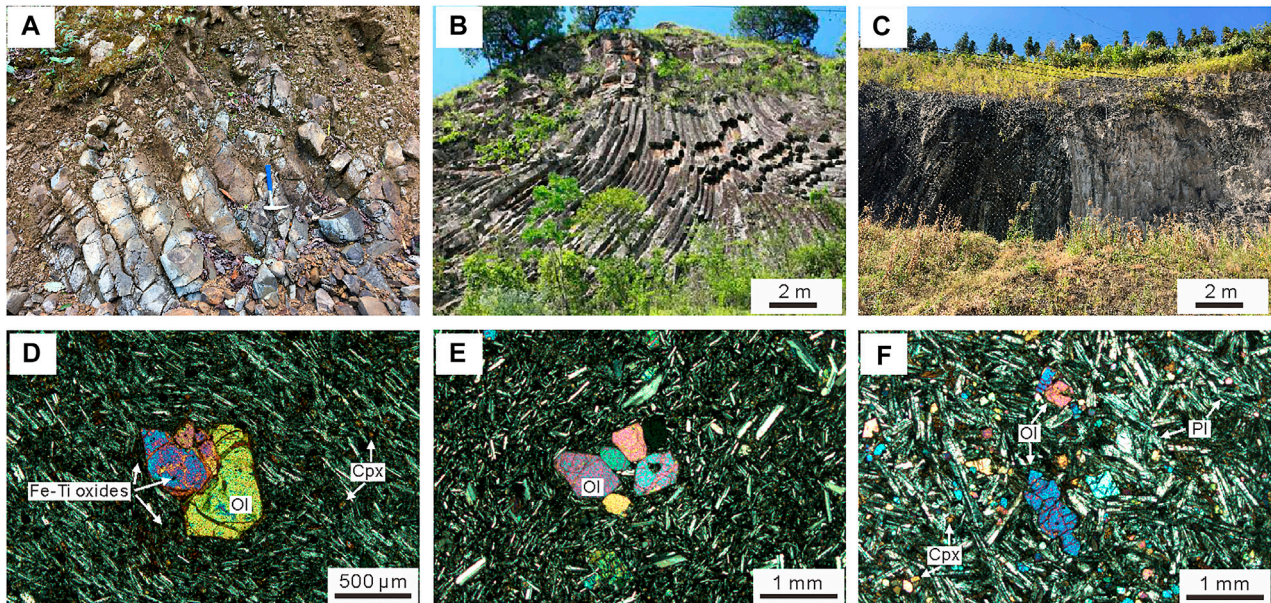
FIGURE 2
Photographs of the Tengchong basalts in the field and photomicrographs under cross-polarized light. **(A)** Columnar jointed basalt in Sudian County in the western area. **(B)** Columnar jointed basalt in Qushi County in the central area. **(C)** Columnar jointed basalt in Tuantian County in the eastern area. **(D)** Euhedral olivine (Ol) phenocrysts in a groundmass containing lath-shaped plagioclase (Pl), clinopyroxene (Cpx) phenocrysts distributed between plagioclase grains, and Fe-Ti oxides distributed in olivine and between plagioclase grains. This photomicrograph is of trachybasalt sample TC20037. **(E)** Euhedral olivine (Ol) phenocrysts in a groundmass containing lath-shaped plagioclases in trachybasalt sample TC20050. **(F)** Olivine and clinopyroxene phenocrysts surrounded by lath-shaped plagioclases in basalt sample TC20042.

dacites, (3) late Pleistocene basalts and trachyandesites, and (4) Holocene basaltic trachyandesites and trachyandesites (Cong et al., 1994; Cheng et al., 2020).

3 Samples and analytical methods

3.1 Samples

Basalts and trachybasalts are mainly distributed in the eastern, western and central areas of the rift basin. A total of 13 samples were collected at the following specific locations: Mangbang, Tuantian, Mengnong, Sudian and Qushi (Figures 1B, Figures 2A–C). All samples were collected from quarries and road cuts, and the samples were of fresh quality. Under microscopic observation, the basalts and trachybasalts are characterized by weak to moderate porphyritic texture (Figures 2D–F), with ~4–6 vol.% olivine, ~3–8 vol.% clinopyroxene, and ~6–10 vol.% plagioclase. The diameters of most olivines range from 100 to 500 μm.

3.2 Whole-rock major and trace elements and Sr-Nd isotopes

Whole-rock major and trace element analyses were carried out at the Key Laboratory of Crustal Dynamics, China Earthquake Administration. Sr and Nd isotopic ratios were analyzed at the Institute of Geochemistry, Chinese Academy of Sciences. The procedure to obtain the whole-rock major and trace element and Sr–Nd isotope data followed Guo et al. (2015). Before conducting the

three types of experiments, the samples were first powdered. The major element contents of basalts were obtained by measuring their loss on ignition (LOI) and oxides. The LOI of the samples was determined after heating the basalt powders at a temperature of 1,000°C. Subsequently, the powders were transformed into fused disks, and major element oxides were analyzed by using Axios-Minerals sequential X-ray fluorescence (XRF) on fused disks. The trace element contents of basalt were examined using inductively coupled plasma–mass spectrometry (ICP–MS) after 4 days of $HF+HNO_3$ digestion. Analytical precisions are generally better than 1% relative for major elements and 5% relative for trace elements. Sr and Nd isotopic ratios were analyzed by using a Neptune Plus mass spectrometer after $HF + HNO_3 + HClO_4$ digestion. The mass fractionation corrections for Sr and Nd isotope ratios were based on $^{86}Sr/^{88}Sr = 0.1194$ and $^{146}Nd/^{144}Nd = 0.7219$, respectively. The analyzed international standard NBS987 had an $^{86}Sr/^{88}Sr$ ratio of 0.710245 ± 0.000016 ($n = 5$), and standard JNdi-1 had a $^{143}Nd/^{144}Nd$ ratio of 0.512117 ± 0.000012 ($n = 5$), which implies good instrument status and accurate testing results.

3.3 Olivine major and trace elements

Major element analysis of olivines was conducted at the East China Institute of Technology. The olivine phenocrysts were manually picked, embedded in epoxy resin and polished on one side for subsequent major and trace element analyses. The major elements of olivine were measured by using a JEOL JXA-8100 electron probe microanalyzer (EPMA). The parameter settings for the experiment were as follows: an acceleration voltage of 15 kV, a beam current of
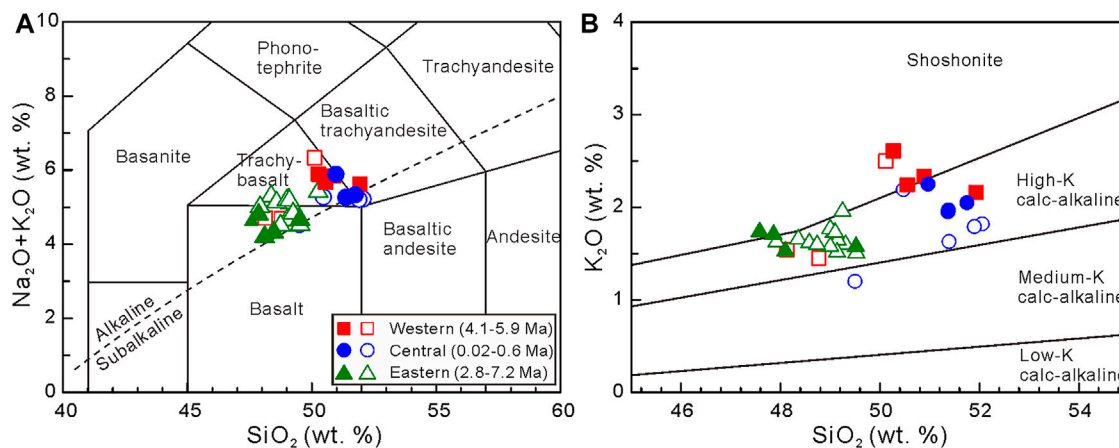
FIGURE 3
Cross-plots of **(A)** Na_2O+K_2O (wt.%) versus SiO_2 (wt.%). The classification boundaries are from Le Bas et al. (1986) and Le Maitre et al. (1986). **(B)** K_2O (wt.%) versus SiO_2 (wt.%) diagram for the Tengchong basalts. The boundaries are from Peccerillo and Taylor (1976) and Rickwood (1989). The filled symbols denote data from this study, and the open symbols are from the literature (Zhang et al., 2012; Zou et al., 2017; Cheng et al., 2018; Tian et al., 2018; Cheng et al., 2020).

20 nA, and a beam diameter of 5 μm. During the measurements, the peak counting time was set to 20 s for major elements (Si, Fe and Mg) and 90 s for minor elements (Mn, Ni, Cr, Ca and Al). After the measurement of every five olivine phenocrysts, an internal olivine standard (MongOl; Batanova et al., 2019) was measured to monitor instrumental drift. According to the analyzed standard and recommended values, the analytical uncertainty is less than 1% for major elements and 5% for minor elements. Olivine major elements are presented in Supplementary Table S2 in Supplementary Information (S1).

Trace elements of olivine were measured by an ELEMENT XR (Thermo Fisher Scientific) inductively coupled plasma–sector field–mass spectrometer coupled with a 193-nm (ArF) Resonetics RESOlution M-50 laser ablation system in the State Key Laboratory of Isotope Geochemistry, Guangzhou Institute of Geochemistry, Chinese Academy of Sciences. The detailed experimental procedure and data reduction strategy are described in Zhang et al. (2019). To analyze olivine trace elements, we set the machine parameters to a laser beam size of 45 μm with a repetition rate of 5 Hz and an energy density of ~4 J cm^{-2}. In addition, the time for the blank collection was 20 s, and the time for signal detection was 30 s. Si was selected as the internal standard element before EPMA analysis. After the measurement of every seven olivine phenocrysts, three United States Geological Survey (USGS) reference glasses, namely, BCR-2G, BHVO-2G and GSD-1G, were examined to correct for time-dependent drift. The measured values of reference glasses agree with the recommended values or the values of previous studies, and the analytical precision was better than 10% for most elements. Olivine trace elements are presented in Supplementary Table S2 in the Supplementary Information (S1).

4 Results

4.1 Whole-rock major and trace elements

Tengchong basalts show relatively low SiO_2 (47.6–52.1 wt.%) and moderate MgO (4.6–9.1 wt.%) and K_2O+Na_2O (4.2–6.3 wt.%)

(Supplementary Table S1 in Supplementary Information (S1)), which plot in the fields of basalts and trachybasalts on the total alkali-silica diagram (Figure 3A). The basalts from the western and eastern areas are slightly more alkaline than those from the central area (Figure 3).

As shown in whole-rock major and trace element covariation diagrams (Figure 4), the Tengchong basalts show negative correlations between MgO and SiO_2, Al_2O_3, and TiO_2, positive correlations between MgO and the Mg number and Ni content, and constant correlations between MgO and CaO contents and CaO/Al_2O_3 ratios.

The pattern of primitive mantle-normalized incompatible trace elements shows positive anomalies in large ion lithophile elements (LILEs, e.g., K, Rb and Ba) and negative anomalies in high field strength elements (HFSEs, Nb, Ta, Zr, Hf and P) (Supplementary Table S1 in Supplementary Information (S1)). The negative Nb-Ta-Ti anomalies and positive Pb anomalies shown in Figure 5A indicate that the Tengchong volcanism is subduction-related. The Tengchong basalts are enriched in light rare earth elements (LREEs). Furthermore, basalts from the central region show higher heavy rare earth elements (HREEs) and lower LREEs than those from the eastern and western regions (Figure 5B).

4.2 Whole-rock Sr–Nd isotopes

The Sr–Nd isotope compositions of the Tengchong basalts are shown in Supplementary Table S1 in the Supplementary Information (S1). The $^{87}Sr/^{86}Sr$ ratios range from 0.705269 to 0.708690, and the $^{143}Nd/^{144}Nd$ ratios range from 0.512359 to 0.512683. In the $^{143}Nd/^{144}Nd$ versus $^{87}Sr/^{86}Sr$ diagram (Figure 6), the samples are located between the EM-I and EM-II endmembers. The $^{87}Sr/^{86}Sr$ ratios of basalts from the central area are similar to those from the western area, and they are lower than those from the eastern area. Integrating previous studies, Figure 6 shows that basalts from the central area generally have relatively lower $^{87}Sr/^{86}Sr$ ratios in the Tengchong volcanic field.
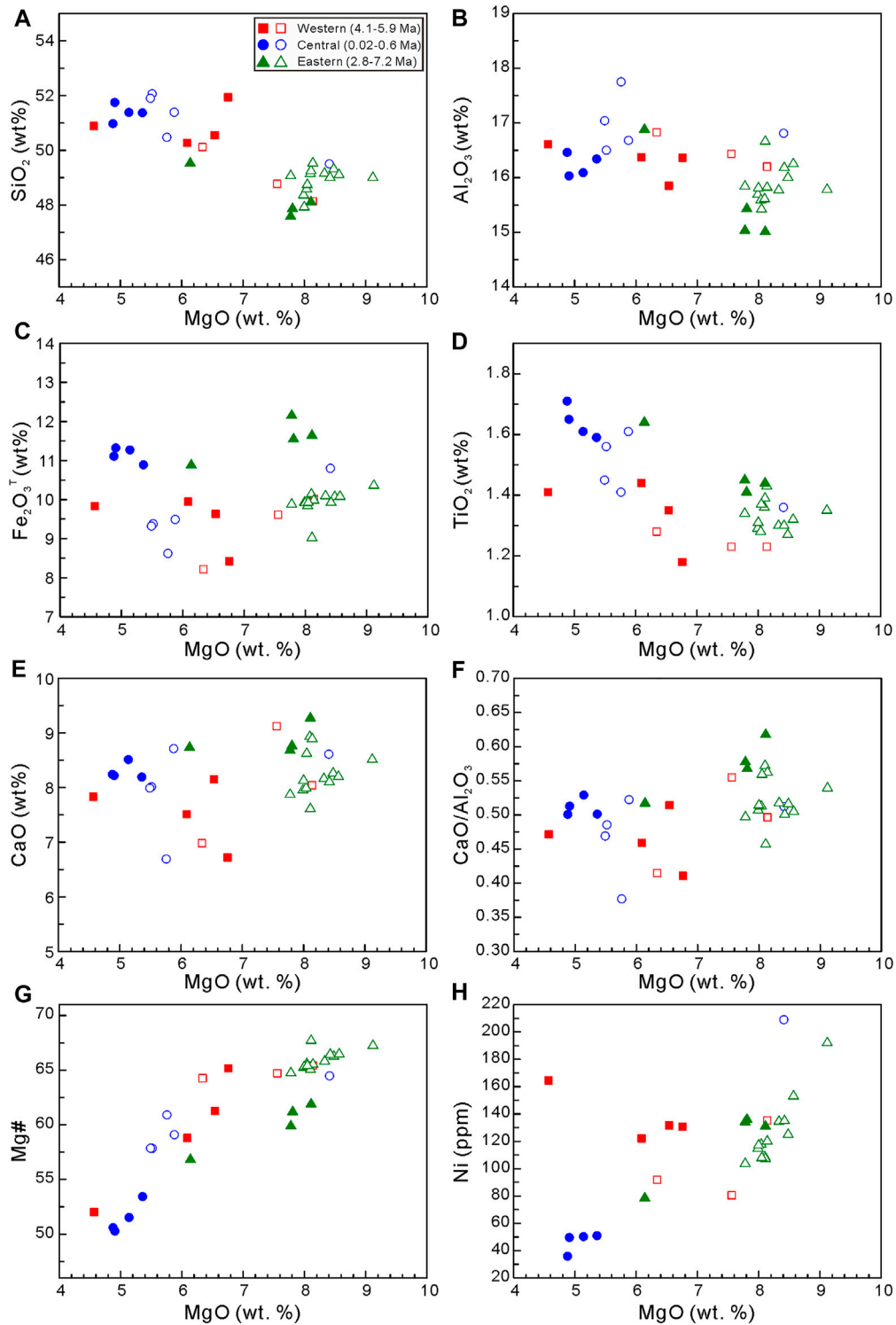
FIGURE 4
(A) SiO$_2$ (wt.%), **(B)** Al$_2$O$_3$ (wt.%), **(C)** total Fe$_2$O$_3$ (wt.%), **(D)** TiO$_2$ (wt.%), **(E)** CaO (wt.%), **(F)** CaO/Al$_2$O$_3$, **(G)** Mg number and **(H)** Ni (ppm) versus MgO (wt.%) for the Tengchong basalts. The filled symbols denote data from this study, and the open symbols are from the literature.

4.3 Major and trace elements in olivine

Olivine in the Tengchong basalts exhibits three main features. First, olivines were generated from the crystallization of magmas. The major and trace elements of olivine are displayed in Supplementary Table S3 in the Supplementary Information (S1). Previous studies have shown that olivine derived from peridotite has low CaO contents (<0.1 wt.%) and that the crystallized from magmas has high CaO contents (>0.1 wt.%) (Simkin and Smith, 1970; Kamenetsky et al., 2006; Wu et al., 2022). Olivine samples from the Tengchong basalts
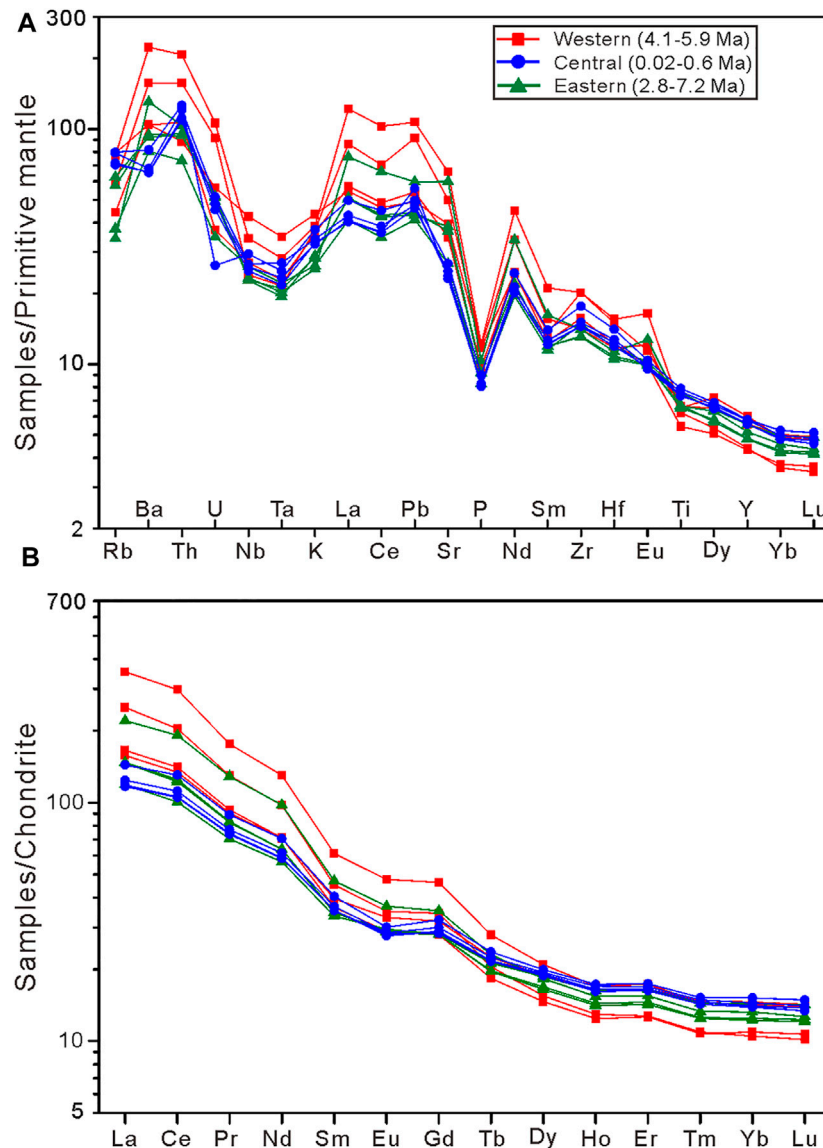
FIGURE 5
(A) Diagram of primitive mantle-normalized trace elements; **(B)** diagram of chondrite-normalized rare Earth elements. The normalization factors are from Sun and McDonough (1989).

display high CaO (0.14–0.35 wt.%) and moderate Fo (75.61–86.21) contents (Supplementary Table S3 in Supplementary Information (S1)). Second, olivine is in equilibrium with its host magmas. Based on the Fe-Mg exchange coefficient $K_D(Fe\text{-}Mg)^{ol\text{-}liq}=0.30 \pm 0.03$ (Roeder and Emslie, 1970), we examine olivine-liquid equilibrium for olivines in the Tengchong basalts (Supplementary Figure S1 in Supplementary Information S2). Although some olivines show variable degrees of olivine crystallization, the data are close to the K_D, indicating olivine-melt equilibrium (Supplementary Figure S1). Third, most olivine phenocrysts in the Tengchong basalts are homogenous. The olivines do not show significant compositional differences from core to rim (Figures 7D–F). In addition, backscattered electron images display consistent color (Figures 7A–C). In this study, we analyze the compositions of olivines to investigate the nature of the mantle source. Previous studies found some olivines showing "bright-white-rim" in backscattered electron

images, indicating composition change from core to rim (Li and Zhang, 2011; Duan et al., 2019). Considering this feature, the cores of olivine contain more information on primary melts, and the compositions of cores in olivines can be used to study the nature of mantle sources (Zhang et al., 2016). Therefore, we only analyze the composition of cores in olivine.

5 Discussion

5.1 Crustal contamination and fractional crystallization

During magma ascent in continental crust, crustal contamination usually affects the elemental and isotopic compositions of continental intraplate volcanic rocks (Li et al., 2016). However, the Tengchong
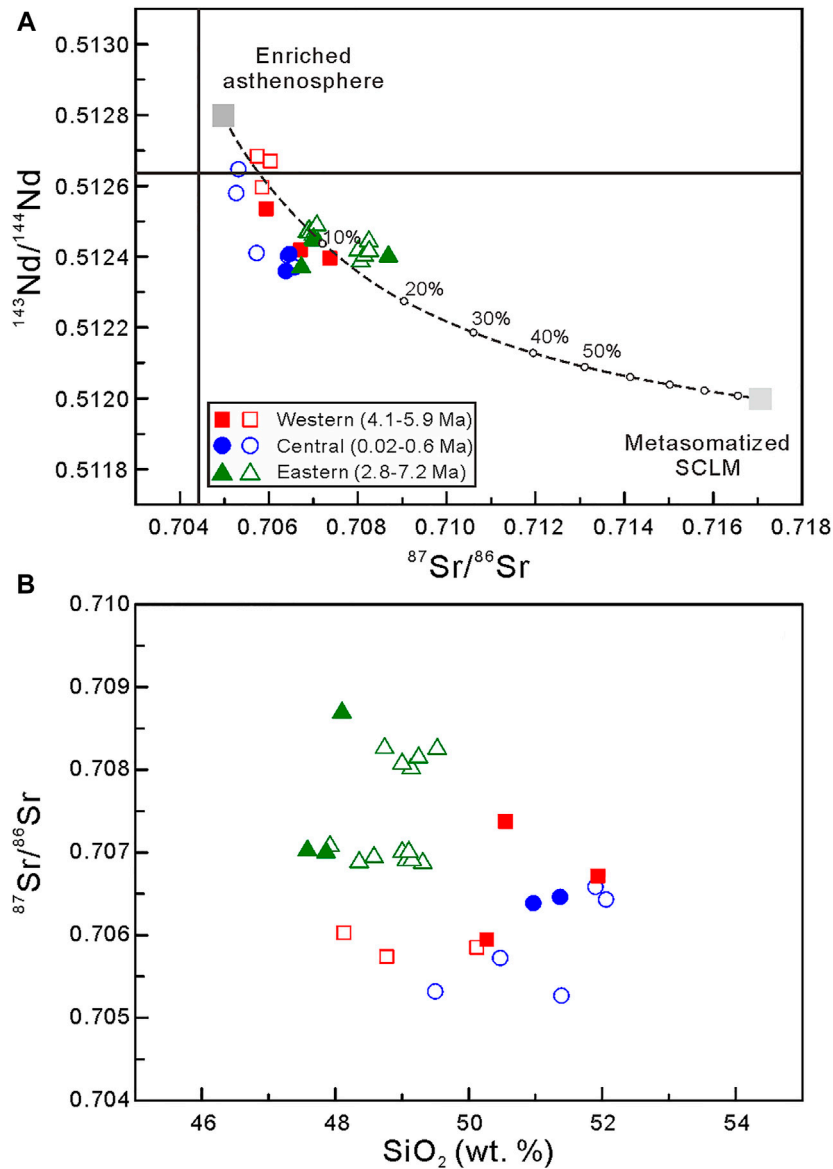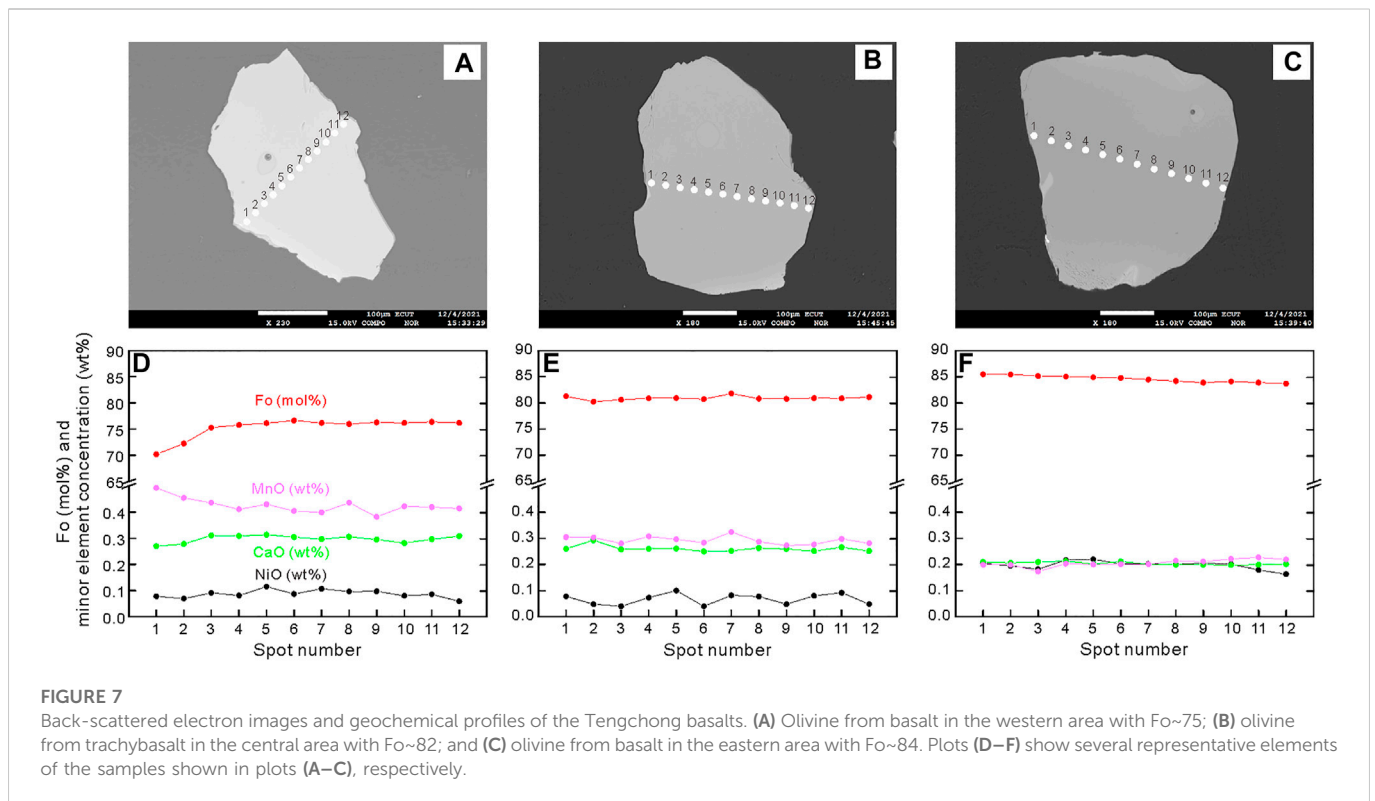
FIGURE 6
(A) Diagram of $^{143}Nd/^{144}Nd$ versus $^{87}Sr/^{86}Sr$; **(B)** diagram of $^{87}Sr/^{86}Sr$ versus SiO_2 for the Tengchong basalts. The isotopic compositions of two geochemical endmembers in plot **(A)** are based on Miller et al. (1999) and Cheng et al. (2020). In plot **(A)**, the dotted curve denotes two-component mixing, and the ratios indicate the percentage of contribution from metasomatized SCLM. The filled symbols denote data from this study, and the open symbols are from the literature.

basalts do not display a positive correlation between $^{87}Sr/^{86}Sr$ and SiO_2 (Figure 6B), suggesting that basalts have not been significantly modified by crustal contamination. Previous studies have also found negligible effects of crustal contamination on the Tengchong basalts (Fan et al., 1999; Zou et al., 2017).

Because the Mg# values range from 50.3 to 67.7, lower than the values of primary magma (Mg# values of 68–75; Frey et al., 1978), the Tengchong magmas experienced evolution. During magma evolution, olivine, clinopyroxene, plagioclase or Fe-Ti oxides may have developed from fractional crystallization in basalts. Olivine crystallization can be verified by two pieces of evidence. First, SiO_2 and Al_2O_3 contents increase and Ni contents decrease with decreasing MgO (Figures 4A, B, H), indicating fractional crystallization of olivine (Lee et al., 2021). Second, constant

$Fe_2O_3^T$ with varying MgO confirms an olivine-controlled fraction in basalts (Zhang et al., 2016) (Figure 4C). The fractional crystallization of the other three minerals is insignificant based on three pieces of evidence. First, crystallization of clinopyroxene is negligible according to nearly constant CaO with decreasing MgO (Figure 4E). Second, crystallization of plagioclase is limited because the positive correlation between Al_2O_3 and MgO contents is absent, and most basalts have Eu′ values >0.88 (Supplementary Table S1 in Supplementary Information (S1)) (Eu′ values ˃0.88 represent little plagioclase fractionation in the Tengchong volcanic field, as suggested by Zou et al. (2017)). Third, Fe_2O_3 and TiO_2 contents do not decrease with decreasing MgO (Figures 4C, D), suggesting little fractional crystallization of Fe-Ti oxides in the Tengchong basalts.

FIGURE 7
Back-scattered electron images and geochemical profiles of the Tengchong basalts. **(A)** Olivine from basalt in the western area with Fo~75; **(B)** olivine from trachybasalt in the central area with Fo~82; and **(C)** olivine from basalt in the eastern area with Fo~84. Plots **(D−F)** show several representative elements of the samples shown in plots **(A−C)**, respectively.
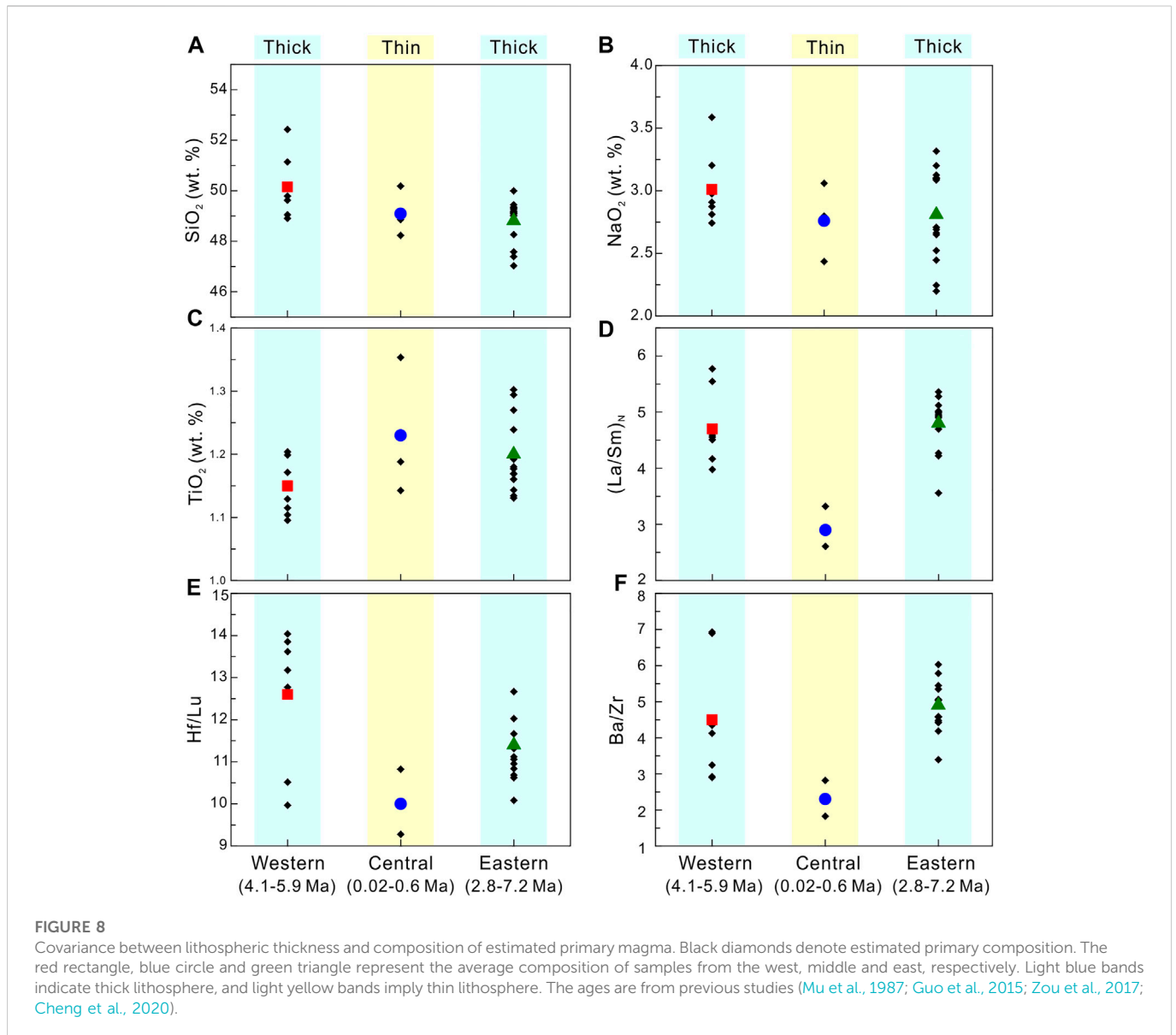
Basalts from the central area show low MgO and Ni contents, suggesting that they are relatively evolved. However, we consider that the olivines in the central area can reflect the information of primary magmas based on three pieces of evidence. First, the Fo values of olivine in the central area range from 80 to 84, which are relatively close to the values of primitive olivine (88–92; Foley et al., 2013). Second, previous studies have found that ^{3}He/^{4}He ratios in olivines from the central area are in the range of MORB, indicating that magmas were generated from asthenospheric melts (Chen et al., 2022). Third, melt inclusions from the central area show lower Th/Yb and higher Nb/U ratios than other melt inclusions from the western and central areas (Supplementary Figure S4), indicating that magmas were generated from a primary mantle source.

According to previous studies, olivines generated from fractional crystallization generally exhibit a trend of decreasing Ni content with decreasing Fo, and mafic magmas that suffer sulfide saturation display sequestration of Ni at the same Fo (e.g., Herzberg, 2011). As shown in Figure 10, olivines from the central area are characterized by lower Ni content than those from the western and the eastern areas at the same Fo. Although this phenomenon can be caused by sulfide saturation, sulfide saturation is negligible. Microscope observations from previous (Zhou et al., 2012) and our studies have not found sulfide in volcanic rocks, suggesting very low amounts of sulfide in magmas. This large variation in Ni contents at the same Fo is likely caused by fractional crystallization. The partition coefficient of Ni is high in silicate melt (Rollision, 1993; Li and Audetat, 2012), and silicate melt is able to affect the Ni content under different melting conditions (Niu et al., 2011). Thus, we consider that the Ni content in olivine can represent the melting conditions and was not affected by sulfide saturation. We conclude that the basaltic elemental and isotopic compositions indicate the nature of the mantle source.

5.2 Asthenosphere–lithosphere interaction and source lithology

It is necessary to investigate the asthenosphere–lithosphere interaction and source lithology for Tengchong magma source before studying the variation in lithospheric thickness. Except for the lithospheric thickness, the lithospheric composition and petrological properties of mantle sources may also affect the chemical composition of basalt and olivine.

Several studies have revealed that the lithospheric mantle and its interaction with the asthenosphere affect the origin of lavas in the Tengchong volcanic field (Zhao and Fan, 2010; Chen et al., 2022). To investigate the contributions of lithospheric mantle and asthenosphere to the magma, we conduct a two-component mixing model in terms of Sr-Nd isotopes. Two endmembers, metasomatized subcontinental lithospheric mantle (SCLM) and enriched asthenospheric mantle, are proposed to form the primary components of the Tengchong volcanic rocks (Chen et al., 2022). According to the mixing model shown in Figure 6, most of the Tengchong basalts plot around the mixing lines and reflect less than 15% of the SCLM contribution (Figure 6). This phenomenon indicates that asthenospheric melts play a dominant role in forming the magmas. Parameters, such as SiO_2 and TiO_2, Na_2O contents and $(La/Sm)_N$, Hf/Lu and Ba/Zr ratios, are used to study the lithosphere thickness. Generally, these parameters in the metasomatized SCLM and enriched asthenospheric mantle exhibit small differences (Supplementary Table S4). Combining the contribution proportion and compositions of two endmembers, the parameters used in the following sections can be used to analyze the nature of the asthenosphere and can be further applied to infer the lithosphere thickness.

FIGURE 8
Covariance between lithospheric thickness and composition of estimated primary magma. Black diamonds denote estimated primary composition. The red rectangle, blue circle and green triangle represent the average composition of samples from the west, middle and east, respectively. Light blue bands indicate thick lithosphere, and light yellow bands imply thin lithosphere. The ages are from previous studies (Mu et al., 1987; Guo et al., 2015; Zou et al., 2017; Cheng et al., 2020).
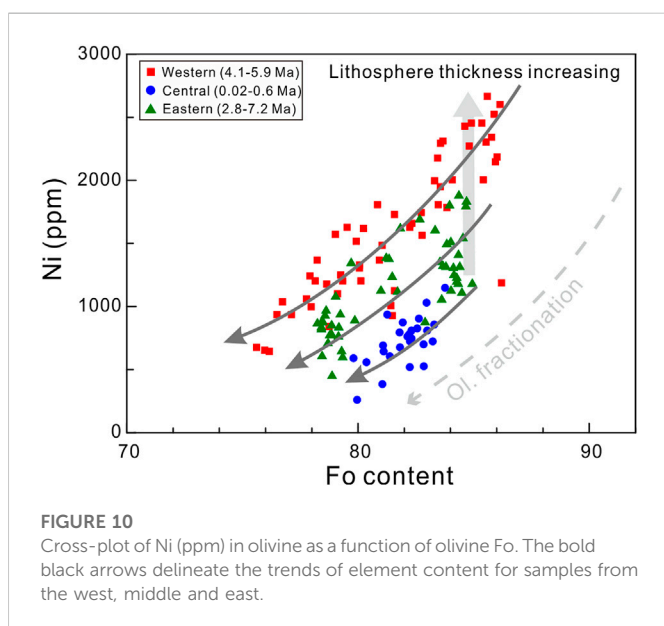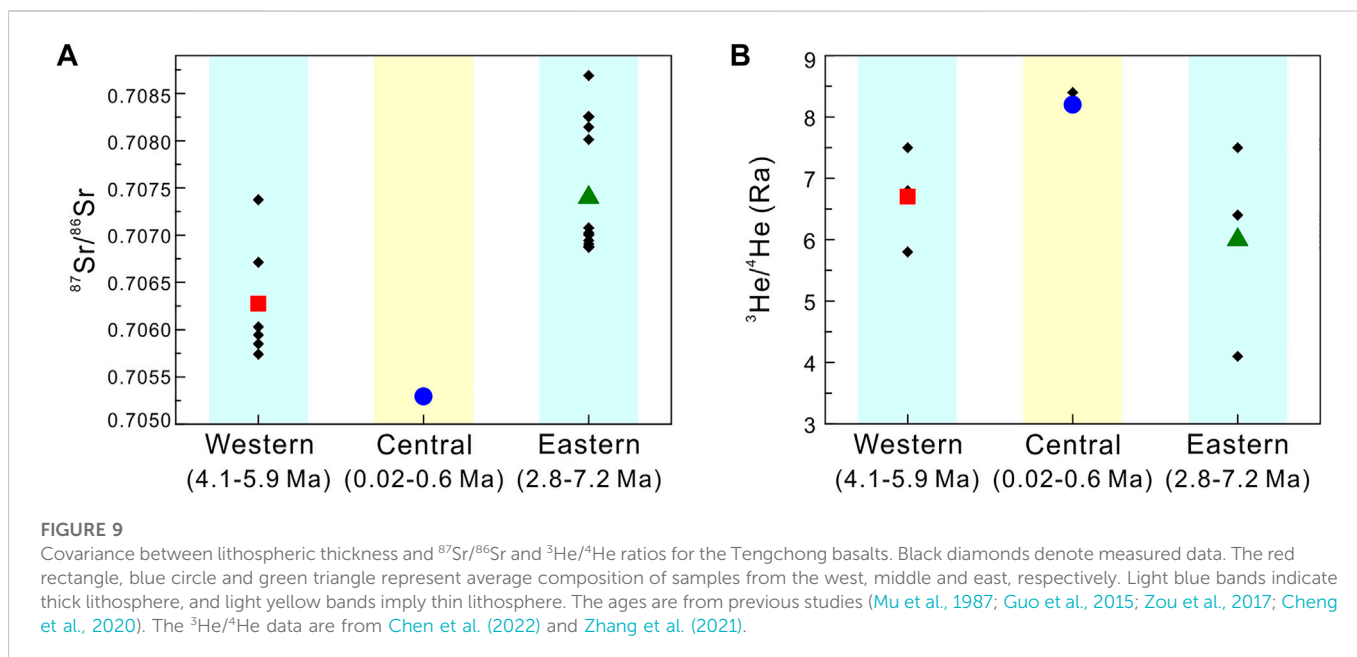
In general, basaltic magmas are formed from the melting of peridotite and pyroxenite components. The pyroxenite component is considered to be related to recycled crustal materials from subducted slab (Sobolev et al., 2007). The element (Mn, Ni, and Ca) contents and ratios (Mn/Fe, Ni/Mg, Ca/Fe and Ni/(Mg/Fe)/1,000) in olivine phenocrysts are used to distinguish the melting of pyroxenite or peridotite (Sobolev et al., 2007; Straub et al., 2008; Rasmussen et al., 2020). Two reasons indicate that the Tengchong basaltic magmas are from the partial melting of a peridotite source. First, Supplementary Figure S2 represents the chemical compositions of olivines in the Tengchong basalts and basalts from other representative zones (Herzberg, 2011). The olivines from the Tengchong basalts display low Ni contents and Fe/Mn ratios and relatively high Mn contents. Their compositions are similar to those of olivines from the Kamchatka and Central American regions, where magmas are from peridotite sources (Ruprecht and Plank 2013; Li et al., 2020). Thus, the Tengchong volcanic rocks may be have been generated from a peridotite source. Second, Mn/Fe does not rely on the process of olivine fractionation, but is mainly controlled by mantle source rocks (Sobolev et al., 2007). Olivines generated from peridotite are

generally characterized by 100×Mn/Fe with values higher than 1.4, which is distinct from the values of pyroxenite ranging from 1.1 to 1.3 (Sobolev et al., 2007). Specifically, olivines from Tengchong basalts show that the 100×Mn/Fe values are mainly larger than 1.4, suggesting the dominant contribution from the peridotite source. In the diagram of Ni/(Mg/Fe)/1,000 versus 100×Mn/Fe, the samples mostly plot close to and overlap with those of olivine crystallized from peridotite-derived melts (Supplementary Figure S3A). In Supplementary Figures S3B, C, the 100×Ni/Mg and 100×Ca/Fe ratios are lower than the peridotitic values owing to fractional crystallization (Kim et al., 2021). Based on the features of olivine compositions, Tengchong basaltic magmas are formed from the partial melting of a peridotite source.

5.3 Variation in lithospheric thickness

Variations in lithospheric thickness can be investigated by the major and trace elements of basalt and olivine (Niu et al., 2011; Gale et al., 2014; Zhang et al., 2016; Liu et al., 2016; Matzen et al., 2017).

FIGURE 9
Covariance between lithospheric thickness and $^{87}Sr/^{86}Sr$ and $^{3}He/^{4}He$ ratios for the Tengchong basalts. Black diamonds denote measured data. The red rectangle, blue circle and green triangle represent average composition of samples from the west, middle and east, respectively. Light blue bands indicate thick lithosphere, and light yellow bands imply thin lithosphere. The ages are from previous studies (Mu et al., 1987; Guo et al., 2015; Zou et al., 2017; Cheng et al., 2020). The $^{3}He/^{4}He$ data are from Chen et al. (2022) and Zhang et al. (2021).

FIGURE 10
Cross-plot of Ni (ppm) in olivine as a function of olivine Fo. The bold black arrows delineate the trends of element content for samples from the west, middle and east.

Based on the estimated primary magmas and measured olivine elemental compositions, we consider that the lithospheric thickness is greater in the western and eastern areas than in the central area of the Tengchong volcanic field.

Primary magmas and olivines can reflect lithospheric thickness. The primary magmas were estimated based on the addition of olivine proposed by Tamura et al. (2014). The composition of the estimated primary magmas of the Tengchong volcanic rocks and the olivine abundance added to the samples are shown in Supplementary Table S2 in the Supplementary Information (S1). Based on the elements and isotopes of primary magmas and olivines shown in Figures 8–9, the lithosphere in the western and eastern areas is probably thicker than that in the central area. This conclusion is drawn according to the following five pieces of evidence.

First, SiO_2 is sensitive to the pressure of melting, and Na_2O and TiO_2 are sensitive to the extent of melting (Langmuir et al., 1992; Gale et al., 2014). Therefore, a thick lithosphere leads to a decrease in SiO_2 and TiO_2 contents and an increase in Na_2O content (Langmuir et al., 1992; Gale et al., 2014). Primary magmas from central to western and eastern areas show a rough decrease in SiO_2 and TiO_2, and an increase in Na_2O (Figures 8A–C). Compared with the SiO_2 content, the correlation is more evident for the TiO_2 and Na_2O contents. These phenomena may suggest a change in lithospheric thickness under the Tengchong volcanic field.

Second, because the Tengchong basaltic magmas formed from the partial melting of a peridotite source, the trace element contents are mainly controlled by the degree of partial melting. As lithospheric thickness is inversely proportional to the degree of partial melting, and $(La/Sm)_N$, Hf/Lu and Ba/Zr ratios increase with decreasing degree of partial melting (Sun et al., 2017; Guo et al., 2020), these trace element ratios are adopted to investigate the change in lithospheric thickness. The basalts from the western and eastern areas show higher ratios of $(La/Sm)_N$, Hf/Lu and Ba/Zr than those from the central area (Figures 8D–F), suggesting thicker lithosphere in the western and eastern areas.

Third, the Sr-He isotopes can partially provide information on lithospheric thickness. Previous studies suggest that the metasomatized SCLM is characterized by high $^{87}Sr/^{86}Sr$ and low $^{3}He/^{4}He$ ratios, and that enriched asthenospheric mantle features relatively low $^{87}Sr/^{86}Sr$ and high $^{3}He/^{4}He$ ratios in the Tengchong volcanic field (Chen et al., 2022). In Figures 9A,B, basalts from the western and eastern areas show lower $^{3}He/^{4}He$ and higher $^{87}Sr/^{86}Sr$ ratios than those from the central area. Basalts from the western and eastern areas display more lithospheric signatures, and those from the central area have more asthenospheric signatures, which can be interpreted as thicker lithosphere in the western and eastern areas.

Fourth, elements in olivine can also be applied to study the variation in lithosphere thickness. According to Niu's model (Niu et al., 2011), the composition of minor elements in olivine relies on the
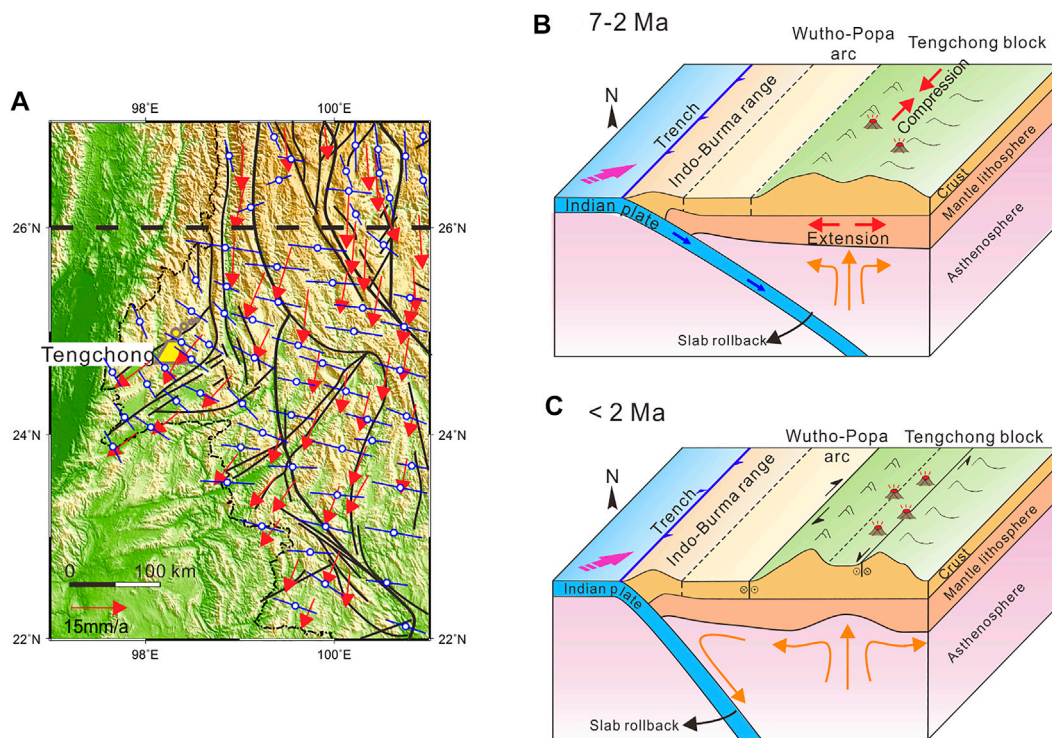
FIGURE 11
(A) Diagrams comparing GPS velocity vectors (red arrows; Wang, 2009) and average XKS fast orientations (blue bars; Gao et al., 2020). The black dashed line (~26°N) shows the inferred transition of mantle anisotropy in this area, and black lines denote major faults. **(B,C)** Schematics of crust–mantle decoupling beneath the Tengchong volcanic field. The eastward underthrusting of the Indian plate following India-Asia collision at 55–50 Ma has resulted in the volcanism in Tengchong at 8 Ma. The crust experienced NNE–NE-oriented compression, while the lithospheric mantle underwent WNW–NW-oriented extension due to slab rollback of the Indian plate (Lee et al., 2016).

variation in lithosphere thickness, which affects the melting process. The lithosphere thickness affects the final depth of melt equilibration, determining the $D^{olivine/melt}$, such as the parameter $Kd_{Ni}^{ol/melt}$ (Niu et al., 2011; Zhang et al., 2016). Several practical studies have applied the Ni content in olivine to investigate the lithospheric thickness (e.g., Walter, 1998; Humphreys and Niu, 2009; Zhang et al., 2016). For the same Fo value, olivine generated under thick lithosphere often exhibits a high Ni concentration. Figure 10 shows that olivines from the western and eastern areas have higher Ni contents than those from the central area, indicating that the thickness of the lithosphere in the western and eastern areas is greater than that in the central area.

Fifth, the study of receiver functions provides direct evidence for the depth of the lithosphere-asthenosphere boundary (LAB) beneath the Tengchong volcanic field. The imaging results show that the depth of the LAB in the central area is 80 km and that in the western and eastern areas is 90 km (Hu et al., 2012; Zhang et al., 2015; Yang et al., 2017).

5.4 Basaltic spatial-temporal variance and geodynamic implications

The basalts in the Tengchong volcanic field were generated from 7.2 Ma to 0.02 Ma (Guo et al., 2015; Zou et al., 2017; Tian et al., 2018). Figure 9 shows clear geochemical variations over the eruption episodes. The basalts that erupted from 2.8 to 7.2 Ma display more lithospheric signatures, and those that formed from 0.02 to 0.6 Ma have more asthenospheric signatures (Chen et al., 2022). The

systematic geochemical variations over time provide evidence that the lithosphere become thinning from the late Miocene to the Holocene. The lithospheric thinning can be caused by lithospheric delamination or lithospheric extension. The lithospheric delamination is less likely, based on the geophysical results. High-resolution seismic tomographic results only show low-velocity anomalies in upper mantle beneath the Tengchong volcanic field, and do not provide any evidence for lithospheric delamination (Lei et al., 2009; Huang et al., 2019; Yao et al., 2021).

In the Tengchong volcanic field, lithospheric extension plays an important role in passive asthenospheric upwelling underground (Chen et al., 2002; Zhou et al., 2012; Guo et al., 2015). During the early stage, the magmas were produced by small degrees of partial melting at high pressures. During the late stage, the lithosphere became thinner, and magmas were produced by large degrees of partial melting at low pressures. The basalts became less alkaline and radiogenic along with lithospheric thinning in the Tengchong volcanic field. This process is similar to extension-related continental volcanism in other areas, where tectonism influences mantle melting and asthenosphere–lithosphere interactions, such as the Basin and Range province and Rio Grande Rift in the United States of America and the Ethiopian volcanic province in Africa (Hart et al., 1989; Thompson and Gibson, 1994; Depaolo and Daley, 2000).

Although lithospheric extension occurred in the Tengchong volcanic field, normal faults did not develop in this area (Wang et al., 2007; Wang et al., 2008). The lack of a normal fault may imply decoupling between the crust and lithospheric mantle. The

extension of the lithosphere usually results in normal faults; for example, in the Basin and Range province and Ethiopian volcanic province, normal faults spread along the rift (Hart et al., 1989; Depaolo and Daley, 2000). However, the Tengchong volcanic field is dominated by strike-slip faults (Wang et al., 2007; Wang et al., 2008). This tectonic phenomenon probably indicates that a compressional regime is dominant in the crust. Therefore, the deformation mechanisms of the crust and lithospheric mantle are different.

Deformation is complex in SE margin of the Tibetan Plateau. It is generally accepted that the lithosphere experienced vertically coherent deformation north of ~26°N, that is curst and lithospheric mantle undergo similar deformation process (Hu et al., 2012; Huang et al., 2015; Gao et al., 2020). However, lithospheric deformation south of ~26°N is intensely debated (Wang et al., 2008; Huang et al., 2015; Shen et al., 2022). From the observation that the fast polarization directions (FPDs) of the XKS are consistent with the orientations of maximum extension in the crust and earthquake focal mechanism solutions, Huang et al. (2015) considered that the crust and lithospheric mantle suffered coherent deformation. That is crust and lithospheric mantle both experienced E–W extension. In addition, based on nearly the same azimuthal anisotropic distributions in the lower crust and uppermost mantle, Shen et al. (2022) inferred consistent deformation of the lithosphere. This means that the crust and lithospheric mantle experienced similar deformation. Many researchers consider the decoupling between the crust and lithospheric mantle south of ~26°N based on the evidence that the directions of the GPS velocity field are generally perpendicular to the FPDs (Flesch et al., 2005; Lev et al., 2006; Sol et al., 2007; Hu et al., 2012; Gao et al., 2020) (Figure 11A). GPS velocity reveals that the crust south of ~26°N undergoes NNE–NE-oriented deformation, while the FPDs (the parameter FPD mainly reflects the deformation of lithosphere) are generally WNW–NW, and imply that lithospheric mantle south of ~26°N must undergo WNW–NW-oriented extension (Gao et al., 2020). Only this pattern of lithospheric deformation can lead to the observed FPDs. The difference between the directions of GPS velocity and FPDs indicates the different deformation patterns in shallow and deep lithosphere.

By integrating previous studies and this study, we constructed the dynamic model shown in Figure 11B to interpret the lithospheric deformation in the Tengchong field. The extrusion of crustal materials from the Tibetan Plateau (Gan et al., 2007) resulted in a compressional regime in SE margin of the Tibetan Plateau. In the Tengchong volcanic field, the crust is under NNE–NE-oriented compression (Wang et al., 2007). The lithospheric mantle undergoes WNW–NW-oriented extension (Wang et al., 2007), which results in the different thicknesses of the lithosphere in the Tengchong volcanic field revealed by our study. We consider that the extension is caused by corner flow in the mantle wedge because of the rollback of the subducting Indian slab in the Burma subduction zone (Hu et al., 2012; Lee et al., 2016). The rollback of the subducting Indian slab is also suggested by Shapiro et al. (2008) based on the mantle structure from seismic tomography.

6 Conclusion

In this study, we found that estimated primary magmas in the eastern and western areas of the Tengchong volcanic field show higher SiO_2, Na_2O, $(La/Sm)_N$, Hf/Lu and Ba/Zr ratios, as well as higher Ni

contents in olivine phenocrysts than those in the central area. These phenomena indicate that the lithosphere in the western and eastern areas is thicker than that in the central area. Combined with the geochronology and characteristics of mantle sources, we find that the lithosphere thins over time in Tengchong. Lithospheric thinning is caused by extension, which may be related to the rollback of the subducting Indian slab. In addition, we consider that the deformations of the crust and lithospheric mantle are different, and our study supports decoupling between the crust and mantle south of ~26°N in SE margin of the Tibetan Plateau.

Data availability statement

The original contributions presented in the study are included in the article/Supplementary Material, further inquiries can be directed to the corresponding author.

Author contributions

KC: Conceptualization, data collection, analysis, investigation, methodology, original draft preparation. SL: Conceptualization, data collection, supervision, project administration, writing—review and editing. DY: Investigation, analysis, funding acquisition. XX: Data collection, funding acquisition, analysis. YW: Analysis. SY: Analysis. SX-Y: Analysis. HZ: Analysis.

Funding

Acknowledgments

Conflict of interest

The author KC was employed by the Research Institute of Petroleum Exploration & Development, PetroChina.

The remaining authors declare that the research was conducted in the absence of any commercial or financial relationships that could be construed as a potential conflict of interest.

Publisher's note

All claims expressed in this article are solely those of the authors and do not necessarily represent those of their affiliated organizations, or those of the publisher, the editors and the reviewers. Any product that may be evaluated in this article, or claim that may be made by its manufacturer, is not guaranteed or endorsed by the publisher.

Supplementary material

The Supplementary Material for this article can be found online at: https://www.frontiersin.org/articles/10.3389/feart.2023.1036001/full#supplementary-material

References

Acocella, V. (2014). Structural control on magmatism along divergent and convergent plate boundaries: Overview, model, problems. *Earth-Science Rev.* 136, 226–288. doi:10.1016/j.earscirev.2014.05.006

Batanova, V. G., Thompson, J. M., Danyushevsky, L. V., Portnyagin, M. V., Garbe Schönberg, D., Hauri, E., et al. (2019). New olivine reference material for *in situ* microanalysis. *Geostand. Geoanalytical Res.* 43 (3), 453–473. doi:10.1111/ggr.12266

Beier, C., Vanderkluysen, L., Regelous, M., Mahoney, J. J., and Garbe-Schonberg, D. G. (2012). Lithospheric control on geochemical composition along the louisville seamount chain. *Geochem. Geophys. Geosystems* 12 (9), 1–19. doi:10.1029/2011gc003690

Chen, F., Satir, M., Ji, J., and Zhong, D. (2002). Nd-Sr-Pb isotopes of Tengchong cenozoic volcanic rocks from Western yunnan, China: Evidence for an enriched-mantle source. *J. Asian Earth Sci.* 21, 39–45. doi:10.1016/s1367-9120(02)00007-x

Chen, H., Xia, Q. K., Ingrin, J., Deloule, E., and Bi, Y. (2017). Heterogeneous source components of intraplate basalts from NE China induced by the ongoing Pacific slab subduction. *Earth Planet. Sci. Lett.* 459, 208–220. doi:10.1016/j.epsl.2016.11.030

Chen, K., He, H., Stuart, F., Liu, S., Xu, X., Cheng, Z., et al. (2022). Binary mixing of lithospheric mantle and asthenosphere beneath Tengchong volcano, SE tibet: Evidence from noble gas isotopic signatures. *Int. Geol. Rev.* 65, 236–252. doi:10.1080/00206814.2022.2042744

Cheng, T., Nebel, O., Sossi, P. A., Wu, J., Siebel, W., Chen, F., et al. (2018). On the Sr-Nd-Pb-Hf isotope code of enriched, Dupal-type sub-continental lithospheric mantle underneath south-Western China. *Chem. Geol.* 489, 46–60. doi:10.1016/j.chemgeo.2018.05.018

Cheng, Z., Guo, Z., Dingwell, D. B., Li, X., Zhang, M., Liu, J., et al. (2020). Geochemistry and petrogenesis of the post-collisional high-K calc-alkaline magmatic rocks in Tengchong, SE Tibet. *J. Asian Earth Sci.* 193, 104309. doi:10.1016/j.jseaes.2020.104309

Cong, B. L., Chen, Q., Zhang, R., Wu, G., and Xu, P. (1994). Petrogenesis of cenozoic volcanic rocks in Tengchong region of Western yunnan province, China. *Sci. China* 37, 1264–1271.

Dai, H. L., Oliveira, B., Zheng, J. P., Griffin, W. L., Afonso, J. C., Xiong, Q., et al. (2021). Melting dynamics of Late Cretaceous lamprophyres in central Asia suggest a mechanism to explain many continental intraplate basaltic suite magmatic provinces. *J. Geophys. Res. Solid Earth* 126 (4), e2021JB021663. doi:10.1029/2021jb021663

Daley, E. E., and Depaolo, D. J. (1992). Isotopic evidence for lithospheric thinning during extension: Southeastern Great Basin. *Geology* 20 (2), 104–108. doi:10.1130/0091-7613(1992)020<0104:iefltd>2.3.co;2

Davies, J. H., and Bunge, H. P. (2006). Are splash plumes the origin of minor hotspots? *Geology* 34 (5), 349–352. doi:10.1130/g22193.1

Depaolo, D. J., and Daley, E. E. (2000). Neodymium isotopes in basalts of the southwest basin and range and lithospheric thinning during continental extension. *Geology* 169, 157–185. doi:10.1016/s0009-2541(00)00261-8

Duan, X., Fan, H., Zhang, H., Yaxley, G., Santosh, M., Tian, H., et al. (2019). Melt inclusions in phenocrysts track enriched upper mantle source for Cenozoic Tengchong volcanic field, Yunnan Province, SW China. *Lithos* 324-325, 180–201. doi:10.1016/j.lithos.2018.10.034

Ellam, R. M. (1992). Lithospheric thickness as a control on basalt geochemistry. *Geology* 20, 153–156. doi:10.1130/0091-7613(1992)020<0153:ltaaco>2.3.co;2

Fan, Q., Liu, R., Wei, H., Shi, L., and Sui, J. (1999). The magmatic evolution of the active volcano in the Tengchong area. *Geol. Rev.* 45, 895–904.

Flesch, L., Holt, W., Silver, P., Stephenson, M., Wang, C., and Chan, W. (2005). Constraining the extent of crust–mantle coupling in central Asia using GPS, geologic, and shear wave splitting data. *Earth Planet. Sci. Lett.* 238, 248–268. doi:10.1016/j.epsl.2005.06.023

Frey, F. A., Green, D. H., and Roy, S. D. (1978). Integrated models of basalt petrogenesis: A study of quartz tholeiites to olivine melilitites from south eastern Australia utilizing geochemical and experimental petrological data. *J. Petrology* 19, 463–513. doi:10.1093/petrology/19.3.463

Foley, S. F., Prelevic, D., Rehfeldt, T., and Jacob, D. E. (2013). Minor and trace elements in olivines as probes into early igneous and mantle melting processes. *Earth and Planetary Science Letters* 363, 181–191.

Gale, A., Langmuir, C. H., and Dalton, C. A. (2014). The global systematics of ocean ridge basalts and their origin. *J. Petrology* 55 (6), 1051–1082. doi:10.1093/petrology/egu017

Gan, W. J., Zhang, P. Z., Shen, Z. K., Niu, Z. J., Wang, M., Wan, Y. G., et al. (2007). Present-day crustal motion within the Tibetan Plateau inferred from GPS measurements. *J. Geophys. Res. Solid Earth* 112 (B8), B08416. doi:10.1029/2005jb004120

Gao, Y., Shi, Y. T., and Wang, Q. (2020). Seismic anisotropy in the southeastern margin of the Tibetan Plateau and its deep tectonic significances. *Chin. J. Geophys.* 63 (3), 802–816. doi:10.6038/cjg2020O0033

Guo, P. Y., Niu, Y. L., Sun, P., Gong, H. M., and Wang, X. H. (2020). Lithosphere thickness controls continental basalt compositions: An illustration using Cenozoic basalts from eastern China. *Geology* 48, 128–133. doi:10.1130/g46710.1

Guo, Z., Cheng, Z., Zhang, M., Zhang, L., Li, X., and Liu, J. (2015). Post-collisional high-K calcalkaline volcanism in Tengchong volcanic field, SE tibet: Constraints on Indian eastward subduction and slab detachment. *J. Geol. Soc.* 172, 624–640. doi:10.1144/jgs2014-078

Hart, W. K., Woldegabriel, G., Walter, R. C., and Mertzman, S. A. (1989). Basaltic volcanism in Ethiopia: Constraints on continental rifting and mantle interactions. *J. Geophys. Res. Solid Earth* 94 (B6), 7731–7748. doi:10.1029/jb094ib06p07731

Hawkesworth, C., Turner, S., Gallagher, K., Hunter, A., Bradshaw, T., and Rogers, N. (1995). Calc-alkaline magmatism, lithospheric thinning and extension in the Basin and Range. *J. Geophys. Res. Solid Earth* 100, 10271–10286. doi:10.1029/94jb02508

Herzberg, C. (2011). Identification of source lithology in the Hawaiian and canary islands: Implications for origins. *J. Petrology* 52 (1), 113–146. doi:10.1093/petrology/egq075

Hoernle, K., White, J. D., Bogaard, P., Hauff, F., Coombs, D. S., Werner, R., et al. (2006). Cenozoic intraplate volcanism on New Zealand: Upwelling induced by lithospheric removal. *Earth Planet. Sci. Lett.* 248 (1), 350–367. doi:10.1016/j.epsl.2006.06.001

Hu, J., Yang, H., Xu, X., Wen, L., and Li, G. (2012). Lithospheric structure and crust-mantle decoupling in the southeast edge of the Tibetan Plateau. *Gondwana Res.* 22 (3), 1060–1067. doi:10.1016/j.gr.2012.01.003

Huang, Z., Wang, L., Xu, M., Ding, Z., Wu, Y., Wang, P., et al. (2015). Teleseismic shear-wave splitting in SE Tibet: Insight into complex crust and upper-mantle deformation. *Earth Planet. Sci. Lett.* 432, 354–362. doi:10.1016/j.epsl.2015.10.027

Huang, Z., Wang, L., Xu, M., Zhao, D., Mi, N., and Yu, D. (2019). PandSWave tomography beneath the SE Tibetan plateau: Evidence for lithospheric delamination. *J. Geophys. Res. Solid Earth* 124, 10292–10308. doi:10.1029/2019jb017430

Huangfu, G., and Jiang, C. (2000). *Study on Tengchong volcanic activities*. Kunming: Yunnan Scientific and Technology Press, 1–418.

Humphreys, E. R., and Niu, Y. L. (2009). On the composition of ocean island basalts (OIB): The effects of lithospheric thickness variation and mantle metasomatism. *Lithos* 112, 118–136. doi:10.1016/j.lithos.2009.04.038

Kamenetsky, V. S., Elburg, M., Arculus, R., and Thomas, R. (2006). Magmatic origin of low-Ca olivine in subduction-related magmas: Co-existence of contrasting magmas. *Chem. Geol.* 233, 346–357. doi:10.1016/j.chemgeo.2006.03.010

Kim, D., Lee, H., Lee, W., Kim, J., Oh, J., Song, J. H., et al. (2021). Helium isotopes and olivine geochemistry of basalts and mantle xenoliths in Jeju Island, South Korea: Evaluation of role of SCLM on the Cenozoic intraplate volcanism in East Asia. *Lithos* 390, 106123. doi:10.1016/j.lithos.2021.106123

King, S. D., and Ritsema, J. (2000). African Hot spot volcanism: Small-scale convection in the upper mantle beneath cratons. *Science* 290, 1137–1140. doi:10.1126/science.290.5494.1137

Kuritani, T., Xia, Q. K., Kimura, J. I., Liu, J., Shimizu, K., Ushikubo, T., et al. (2019). Buoyant hydrous mantle plume from the mantle transition zone. *Sci. Rep.* 9, 6549. doi:10.1038/s41598-019-43103-y

Langmuir, C. H., Klein, E. M., and Plank, T. (1992). "Petrological systematics of midocean ridge basaltsçConstraints on melt generation beneath ocean ridges," in

Mantle flow and melt generation at mid-ocean ridges. Editors J. Phipps Morgan, D. K. Blackman, and J. M. Sinton (Washington DC: American Geophysical Union), 183–280.

Le Bas, M. J., Le Maitre, R. W., Sterckeisen, A., and Zanettin, B. A. (1986). A chemical classification of volcanic rocks based on the total alkali-silica diagram. *J. Petrology* 27 (3), 745–750. doi:10.1093/petrology/27.3.745

Le Maitre, R. W. A., Zanettin, B., Le Bas, M. J., Bonin, B., and Bateman, P. (1986). *A classification of igneous rocks and glossary of terms: Recommendations of the international union of geological Sciences subcommission on the systematics of igneous rocks*. Oxford and Blackwell: Cambridge University.

Lee, H. Y., Chung, S. L., and Yang, H. M. (2016). Late Cenozoic volcanism in central Myanmar: Geochemical characteristics and geodynamic significance. *Lithos* 245, 174–190. doi:10.1016/j.lithos.2015.09.018

Lee, W., Lee, H., Kim, D., Kim, J., Oh, J., Song, J., et al. (2021). Trace element and helium isotope geochemistry of the Cenozoic intraplate volcanism in the East Sea (Sea of Japan): Implications for lithosphere-asthenosphere interaction. *Lithos* 388-389, 106075. doi:10.1016/j.lithos.2021.106075

Lei, J., Zhao, D., and Su, Y. (2009). Insight into the origin of the Tengchong intraplate volcano and seismotectonics in southwest China from local and teleseismic data. *J. Geophys. Res.* 114, B05302. doi:10.1029/2008jb005881

Lev, E., Long, M. D., and Vanderhilst, R. (2006). Seismic anisotropy in Eastern Tibet from shear wave splitting reveals changes in lithospheric deformation. *Earth Planet. Sci. Lett.* 251, 293–304. doi:10.1016/j.epsl.2006.09.018

Li, J., Niu, Y., Hu, Y., Chen, S., Zhang, Y., Duan, M., et al. (2016). Origin of the late early cretaceous granodiorite and associated dioritic dikes in the hongqilafu pluton, northwestern Tibetan plateau: A case for crust-mantle interaction. *Lithos* 260, 300–314. doi:10.1016/j.lithos.2016.05.028

Li, N., and Zhang, L. Y. (2011). A study on volcanic minerals and hosted melt inclusions in newly-erupted Tengchong volcanic rocks, Yunnan Province. *Acta Petrol. Sin.* 27 (10), 2842–2854.

Li, X. H., Zeng, Z. G., Dan, W., Yang, H. X., Wang, X. Y., Fang, B. W., et al. (2020). Source lithology and crustal assimilation recorded in low $\delta^{18}O$ olivine from Okinawa Trough, back-arc basin. *Lithos* 360, 105444. doi:10.1016/j.lithos.2020.105444

Li, Y., and Audétat, A. (2012). Partitioning of V, Mn, Co, Ni, Cu, Zn, As, Mo, Ag, Sn, Sb, W, Au, Pb, and Bi between sulfide phases and hydrous basanite melt at upper mantle conditions. *Earth Planet. Sci. Lett.* 355, 327–340. doi:10.1016/j.epsl.2012.08.008

Liu, J. Q., Chen, L. H., Zeng, G., Wang, X. J., Zhong, Y., Yu, X., et al. (2016). Lithospheric thickness controlled compositional variations in potassic basalts of Northeast China by melt-rock interactionsThe roles of pyroxenite and peridotite in the mantle sources of oceanic basalts. *Geophys. Res. Lett. Geoscience* 4310 (67), 2582530–2589535. doi:10.1038/ngeo2968

Matzen, A. K., Wood, B. J., Baker, M. B., Stolper, E. M., et al. (2017). The roles of pyroxenite and peridotite in the mantle sources of oceanic basalts. *Nature Geoscience* 10 (7), 530–535.

McKenzie, D., and Bickle, M. (1988). The volume and composition of melt generated by extension of the lithosphere. *J. Petrology* 29, 625–679. doi:10.1093/petrology/29.3.625

Miller, C., Schuster, R., Klötzli, U., Frank, W., and Purtscheller, F. (1999). Post-Collisional potassic and ultrapotassic magmatism in SW tibet: Geochemical and Sr–Nd–Pb–O isotopic constraints for mantle source characteristics and petrogenesis. *J. Petrology* 40 (9), 1399–1424. doi:10.1093/petroj/40.9.1399

Mo, X., Zhao, Z., Deng, J., Flower, M. F. J., Yu, X., Luo, Z., et al. (2006). "Petrology and geochemistry of postcollisional volcanic rocks from the Tibetan plateau: Implications for lithosphere heterogeneity and collision-induced asthenospheric mantle flow," in *Postcollisional tectonics and magmatism in the mediterranean region and asia*. Editors J. S. Nie, B. K. Horton, and G. D. Hoke (Colorado: Geological Society of America Special Papers), 507–530.

Mu, Z., Tong, W., and Curtis, G. H. (1987). Times of volcanic activity and origin of magma in Tengchong geothermal area, west Yunnan province. *Acta Geophys. Sin.* 30, 261–270.

Niu, Y. L. (2021). Lithosphere thickness controls the extent of mantle melting, depth of melt extraction and basalt compositions in all tectonic settings on Earth – a review and new perspectives. *Earth-Science Rev.* 217, 103614. doi:10.1016/j.earscirev.2021.103614

Niu, Y. L., Wilson, M., Humphreys, E. R., and O'Hara, M. J. (2011). The origin of intra-plate ocean island basalts (OIB): The lid effect and its geodynamic implications. *J. Petrology* 52, 1443–1468. doi:10.1093/petrology/egr030

Özdemir, Y., and Güleç, N. (2014). Geological and geochemical evolution of the quaternary süphan stratovolcano, eastern anatolia, Turkey: Evidence for the lithosphere–asthenosphere interaction in post-collisional volcanism. *J. Petrology* 55 (1), 37–62. doi:10.1093/petrology/egt060

Peccerillo, A., and Taylor, S. R. (1976). Geochemistry of Eocene calc-alkaline volcanic rocks from the Kastamonu area, northern Turkey. *Contributions Mineralogy Petrology* 58 (1), 63–81. doi:10.1007/bf00384745

Rasmussen, M. B., Halldórsson, S. A., Gibson, S. A., and Guðfinnsson, G. H. (2020). Olivine chemistry reveals compositional source heterogeneities within a tilted mantle plume beneath Iceland. *Earth Planet. Sci. Lett.* 531, 116008. doi:10.1016/j.epsl.2019.116008

Rickwood, P. C. (1989). Boundary lines within petrologic diagrams which use oxides of major and minor elements. *Lithos* 22 (4), 247–263. doi:10.1016/0024-4937(89)90028-5

Roeder, P. L., and Emslie, R. F. (1970). Olivine–liquid equilibrium. *Contributions Mineralogy Petrology* 29, 275–289. doi:10.1007/bf00371276

Rollinson, H. (1993). *Using geochemical data: Evaluation, presentation, interpretation*. Harlow, UK: Longman, p88.

Ruprecht, P., and Plank, T. (2013). Feeding andesitic eruptions with a high-speed connection from the mantle. *Nature* 500, 68–72. doi:10.1038/nature12342

Shapiro, N. M., Ritzwoller, M. H., and Engdahl, E. R. (2008). Structural context of the great Sumatra-Andaman Islands earthquake. *Geophys. Res. Lett.* 35, L05301. doi:10.1029/2008gl033381

Shen, W., Liu, S., Xu, X., Yang, D., Wang, W., Wu, Y., et al. (2022). The crustal and uppermost mantle dynamics of the Tengchong-Baoshan region revealed by P-wave velocity and azimuthal anisotropic tomographyMinor-element distribution in olivine. *Geophys. J. Int. J. Geol.* 78, 304–325. doi:10.1086/627519

Simkin, T., and Smith, J. V. (1970). Minor-element distribution in olivine. *J. Geol.* 78, 304–325.

Sobolev, A. V., Hofmann, A. W., Kuzmin, D. V., Yaxley, G. M., Arndt, N. T., Chung, S. L., et al. (2007). The amount of recycled crust in sources of mantle-derived melts. *Science* 316 (5823), 412–417. doi:10.1126/science.1138113

Sol, S., Meltzer, A., Bürgmann, R., van der Hilst, R. D., King, R., Chen, Z., et al. (2007). Geodynamics of the southeastern Tibetan Plateau from seismic anisotropy and geodesy. *Geology* 35, 563–566. doi:10.1130/g23408a.1

Straub, S. M., LaGatta, A. B., Martin-Del Pozzo, A. L., Langmuir, C. H., et al. (2008). Evidence from high-Ni olivines for a hybridized peridotite/pyroxenite source for orogenic andesites from the central Mexican Volcanic Belt. *Geochemistry, Geophysics, Geosystems* 9, Q03007. doi:10.1029/2007GC001583

Sun, P., Niu, Y. L., Guo, P. Y., Ye, L., Liu, J. J., and Feng, Y. X. (2017). Elemental and Sr-Nd-Pb isotope geochemistry of the Cenozoic basalts in Southeast China: Insights into their mantle sources and melting processes. *Lithos* 272-273, 16–30. doi:10.1016/j.lithos.2016.12.005

Sun, S. S., and McDonough, W. F. (1989). Chemical and isotopic systematics of oceanic basalts: Implications for mantle composition and processes. *Geol. Soc. Lond. Spec. Publ.* 42 (1), 313–345. doi:10.1144/gsl.sp.1989.042.01.19

Tamura, Y., Ishizuka, O., Stern, R. J., Nichols, A. R. L., Kawabata, H., Hirahara, Y., et al. (2014). Mission immiscible: Distinct subduction components generate two primary magmas at pagan volcano, mariana arc. *J. Petrology* 55, 63–101. doi:10.1093/petrology/egt061

Tang, Y. J., Zhang, H. F., and Ying, J. F. (2006). Asthenosphere–lithospheric mantle interaction in an extensional regime: Implication from the geochemistry of cenozoic basalts from taihang mountains, north China craton. *Chem. Geol.* 233 (3-4), 309–327. doi:10.1016/j.chemgeo.2006.03.013

Thompson, R. N., and Gibson, S. A. (1994). Magmatic expression of lithospheric thinning across continental rifts. *Tectonophysics* 233, 41–68. doi:10.1016/0040-1951(94)90219-4

Tian, H., Yang, W., Li, S., Ke, S., and Duan, X. (2018). Low $\delta^{26}Mg$ volcanic rocks of Tengchong in southwestern China: A deep carbon cycle induced by supercritical liquids. *Geochimica Cosmochimica Acta* 240, 191–219. doi:10.1016/j.gca.2018.08.032

Timm, C., Hoernle, K., Van Den Bogaard, P., Bindeman, I., and Weaver, S. (2009). Geochemical evolution of intraplate volcanism at banks peninsula, New Zealand: Interaction between asthenospheric and lithospheric melts. *J. Petrology* 50, 989–1023. doi:10.1093/petrology/egp029

Walter, M. J. (1998). Melting of garnet peridotite and the origin of komatiite and depleted lithosphere. *J. Petrology* 39, 29–60. doi:10.1093/petroj/39.1.29

Wang, C. Y., Flesch, L. M., Silver, P. G., Chang, L. J., and Chan, W. W. (2008b). Evidence for mechanically coupled lithosphere in central Asia and resulting implications. *Geology* 36, 363–366. doi:10.1130/g24450a.1

Wang, E. Q., and Burchfiel, B. C. (1997). Interpretation of cenozoic tectonics in the right-lateral accommodation zone between the ailao Shan shear zone and the eastern himalayan syntaxis. *Int. Geol. Rev.* 39, 191–219. doi:10.1080/00206819709465267

Wang, G., Wan, J., Wang, E., Zhang, D., and Li, F. (2008a). Late Cenozoic to recent transtensional deformation across the Southern part of the Gaoligong shear zone between the Indian plate and SE margin of the Tibetan plateau and its tectonic origin. *Tectonophysics* 460, 1–20. doi:10.1016/j.tecto.2008.04.007

Wang, M. (2009). *Analysis of GPS data with high precision and study on present-day crustal deformation in China*. Beijing: Institute of Geology, China Earthquake Administration, 1–95.

Wang, Y., Zhang, X., Jiang, C., Wei, H., and Wan, J. (2007). Tectonic controls on the late Miocene–Holocene volcanic eruptions of the Tengchong volcanic field along the southeastern margin of the Tibetan plateau. *J. Asian Earth Sci.* 30, 375–389. doi:10.1016/j.jseaes.2006.11.005

White, R. S., Spence, G. D., Fowler, S. R., McKenzie, D. P., Westbrook, G. K., and Bowen, A. N. (1987). Magmatism at rifted continental margins. *Nature* 330, 439–444. doi:10.1038/330439a0

Wu, Y. D., Yang, J. H., Stagno, V., Nekrylov, N., Wang, J. T., and Wang, H. (2022). Redox heterogeneity of picritic lavas with respect to their mantle sources in the Emeishan large igneous province. *Geochimica Cosmochimica Acta* 320, 161–178. doi:10.1016/j.gca.2022.01.001

Xu, J. Y., Giuliani, A., Li, Q. L., Lu, K., Melgarejo, J. C., and Griffin, W. L. (2021). Light oxygen isotopes in mantle-derived magmas reflect assimilation of sub-continental

lithospheric mantle material. *Nat. Commun.* 12 (1), 6295–6313. doi:10.1038/s41467-021-26668-z

Xu, Y. G., Blusztajn, J., Ma, J. L., Suzuki, K., Liu, J. F., and Hart, S. R. (2008). Late archean to early proterozoic lithospheric mantle beneath the Western north China craton: Sr–Nd–Os isotopes of peridotite xenoliths from yangyuan and fansi. *Lithos* 102 (1-2), 25–42. doi:10.1016/j.lithos.2007.04.005

Yang, H., Peng, H., and Hu, J. (2017). The lithospheric structure beneath southeast Tibet revealed by P and S receiver functions. *J. Asian Earth Sci.* 138, 62–71. doi:10.1016/j.jseaes.2017.02.001

Yao, J., Liu, S., Wei, S., Hubbard, J., Huang, B., Chen, M., et al. (2021). Slab models beneath central Myanmar revealed by a joint inversion of regional and teleseismic traveltime data. *J. Geophys. Res. Solid Earth* 126, e2020JB022164. doi:10.1029/2020jb020164

Zhang, L., Hu, Y., Qin, M., Duan, Y., Duan, Y. Z., Peng, H. C., et al. (2015). Study on crustal and lithosphere thicknesses of Tengchong volcanic area in Yunnan. *Chin. J. Geophys.* 58 (3), 256–268. doi:10.1002/cjg2.220171

Zhang, L., Ren, Z. Y., Xia, X. P., Yang, Q., Hong, L. B., and Wu, D. (2019). *In situ* determination of trace elements in melt inclusions using laser ablation-inductively coupled plasma-sector field-mass spectrometry. *Rapid Commun. Mass Spectrom.* 33, 361–370. doi:10.1002/rcm.8359

Zhang, L. Y., Prelevic, D., Li, N., Mertz-Kraus, R., and Buhre, S. (2016). Variation of olivine composition in the volcanic rocks in the songliao basin, NE China: Lithosphere control on the origin of the K-rich intraplate mafic lavas. *Lithos* 262, 153–168. doi:10.1016/j.lithos.2016.06.028

Zhang, M., and Guo, Z. (2016). Origin of Late Cenozoic Abaga–Dalinuoer basalts, eastern China: Implications for a mixed pyroxenite–peridotite source related with deep subduction of the Pacific slab. *Gondwana Res.* 37, 130–151. doi:10.1016/j.gr.2016.05.014

Zhang, M., Xu, S., Zhou, X., Caracausi, A., Sano, Y., Guo, Z., et al. (2021). Deciphering a mantle degassing transect related with India-Asia continental convergence from the perspective of volatile origin and outgassing. *Geochimica Cosmochimica Acta* 310, 61–78. doi:10.1016/j.gca.2021.07.010

Zhang, Y., Liu, J., and Meng, F. (2012). Geochemistry of cenozoic volcanic rocks in Tengchong, SW China: Relationship with the uplift of the Tibetan plateau. *Isl. Arc* 21 (4), 255–269. doi:10.1111/j.1440-1738.2012.00819.x

Zhao, Y., and Fan, Q. (2010). Magma origin and evolution of Maanshan volcano, Dayingshan volcano and Heikongshan volcano in Tengchong area. *Acta Petrol. Sin.* 26, 1133–1140.

Zhou, M., Robinson, P., Wang, C., Zhao, J., Yan, D., Gao, J., et al. (2012). Heterogeneous mantle source and magma differentiation of quaternary arc-like volcanic rocks from Tengchong, SE margin of the Tibetan Plateau. *Contributions Mineralogy Petrology* 163 (5), 841–860. doi:10.1007/s00410-011-0702-8

Zhu, B., Mao, C., Lugmair, G. W., and Macdougall, J. D. (1983). Isotopic and geochemical evidence for the origin of Plio-Pleistocene volcanic rocks near the Indo-Eurasian collisional margin at Tengchong, China. *Earth Planet. Sci. Lett.* 65 (2), 263–275. doi:10.1016/0012-821x(83)90165-6

Zhu, R. X., Yang, J. H., and Wu, F. Y. (2012). Timing of destruction of the north China craton. *Lithos* 149, 51–60. doi:10.1016/j.lithos.2012.05.013

Zou, H., Ma, M., Fan, Q., Xu, B., Li, S., Zhao, Y., et al. (2017). Genesis and open-system evolution of Quaternary magmas beneath southeastern margin of Tibet: Constraints from Sr-Nd-Pb-Hf isotope systematics. *Lithos* 272, 278–290. doi:10.1016/j.lithos.2016.12.012